First germanium doped titanium disulfide polytypes Crystal structure and metal–metal interactions

L. Hammoudi, A. Gómez-Herrero, M. Kars, T. Roisnel, L.C. Otero-Diáz

Abbreviations

CVT: Chemical Vapor Transport

2D: Two Dimensional

TMDCs: Transition Metal Dichalcogenides

SRO: Short Range Order

SAED: Selected Area Electron Diffraction

TEM: Transmission Electron Microscopy

HRTEM: High Resolution Transmission Electron Microscopy

HAADF: High Angle Annular Dark Field

STEM: Scanning Transmission Electron Microscopy

XEDS: X-Ray Energy Dispersive Spectroscopy

XRD: X-Ray Diffraction

ADP's: Anisotropic Displacement Parameters

BVS: Bond Valance Sum.

First Germanium Doped Titanium Disulfides Polytypes :
Crystal Structure and Metal-Metal Interactions

Premier Dopage au Germanium de Polytypes de disulfure de Titane :
Structure Cristalline et Interactions Métal-Métal

Lamia Hammoudi [a], *Adrian Gómez-Herrero* [b], *Mohammed Kars* [a*], *Thierry Roisnel* [c], *Luis Carlos Otero-Diáz* [b,d].

[a] *Faculté de Chimie, Laboratoire Sciences des Matériaux, USTHB, BP32 16000 Alger Algérie*

[b] *Centro de Microscopia Electrónica, Universidad Complutense, 28040 Madrid Spain.*

[c] *Centre de Diffractométrie X Sciences Chimiques de Rennes UMR 6226 CNRS Université de Rennes 1 Campus de Beaulieu Avenue du Général Leclerc France.*

[d] *Dpto. Inorgánica, Fac. C.C. Químicas, Universidad Complutense, 28040 Madrid Spain.*

Abstract

Single crystals of Ge-doped TiS_2 polytypes, 1T, $(4H)_2$, 12R, and their corresponding new $a\sqrt{3} \times a\sqrt{3}$ superstructure were grown by chemical vapor transport method. The crystals were characterized by combining X-ray diffraction and transmission electron microscopy techniques. The structures of these polytypes are all based on close packing layers of sulfur of CdI_2-type structure. Except in the 1T polytype, the germanium atoms are observed to be equally distributed over both partial and complete occupancy layers. A significant distortion of the metal–sulfur distances is observed in the superstructure polytypes, as a consequence of metal–metal corrugated layers. The 12R-$a\sqrt{3} \times a\sqrt{3}$ superstructure is revealed by both electron diffraction and X-ray diffraction by the presence of satellite reflections. Electron diffraction patterns from the 12R polytype show highly structured diffuse scattering surrounding the main spots. These diffuse segments, which are arranged in triangles sharing vertices, correspond to a $2a^* \times 2a^*$ superstructure and are attributed to the short-range order of metal atoms in the partially filled layers.

Résumé

La croissance des monocristaux des polytypes de TiS_2 dopés au germanium, 1T, (4H)2, 12R, et de sa nouvelle superstructure $a\sqrt{3} \times a\sqrt{3}$ correspondante a été réalisée par la méthode du transport chimique en phase vapeur (CVT). Les cristaux ont été caractérisés en combinant les techniques de diffraction des rayons X (DRX) et de la microscopie électronique à transmission (MET). La structure de ces polytypes est basée sur des couches compactes de soufre de type CdI2. À l'exception du polytype-1T, les atomes de germanium sont répartis de manière équitable à la fois dans les couches partiellement ou totalement occupées. Une

importante distorsion est observée dans les distances métal–soufre des polytypes à superstructure, résultat de l'ondulation des couches métal–métal. La superstructure 12R-$a\sqrt{3} \times a\sqrt{3}$ a été identifiée à la fois par diffraction des rayons X et par microscopie électronique par la présence de réflexions satellites. Les clichés de diffraction électronique du polytype 12R montrent une diffusion diffuse très structurée entourant les taches (*spots*) de diffraction principales. Cette diffusion en forme de segments triangulaires se partageant des sommets correspond à une superstructure $2a^* \times 2a^*$ et est attribuée à un ordre à courte distance (SRO) des atomes métalliques dans les couches métalliques partiellement occupées.
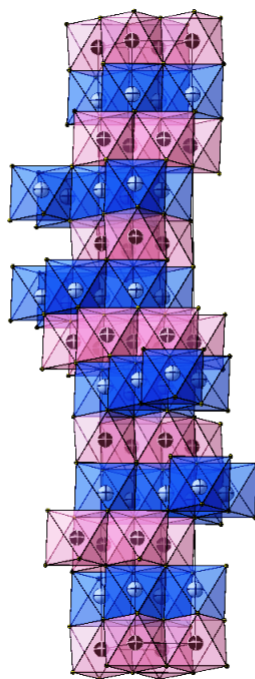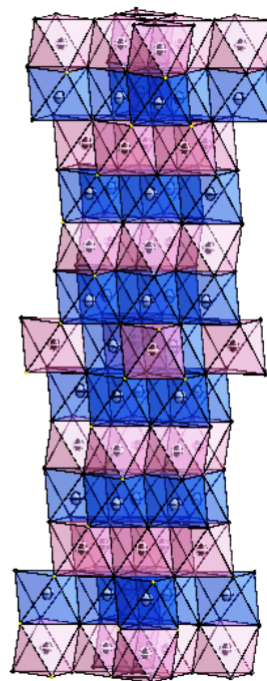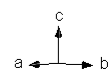
Graphical abstract
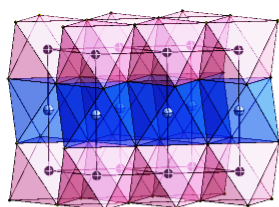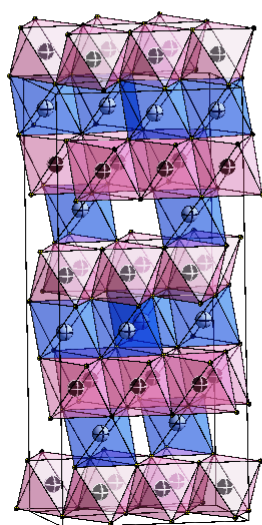
1. Introduction

Titanium disulphide TiS_2 belongs to the layered transition metal dichalcogenides (TMDCs) family, which has been widely studied for decades because of the variety of their electronic properties [1-2].

After the discovery of graphene and the advance of new synthetic methods, renewed interest has been focused on 2D (two dimensional) M-dopped TMDCs (M = transition metal) for their new potential applications (see [3-7] and references therein for recent results).

TiS_2 [8] and its intercalation compounds have been intensively studied and shown to be promising cathode materials in rechargeable batteries [9] and as potential hydrogen storage materials [10].

The most salient features of the $Ti_{1+x}S_2$ system are its surprising capacity for adopting various structures and their coexistence, the polytypism, nonstoichiometry and order/disorder phenomena [11-12]. Various morphologies of TiS_2 such as nanotubes [13-14] and fullerenelike [15], have been successfully synthesized. This complexity appears to be a specific property of the titanium-sulphur atomic pair with no equivalent in other systems [16].

Polytypism in TiS_2 was observed by Tronc et al., and Legendre et al. [17, 18], with different periodicities along the c axis. The structures of these polytypes are all based on close -packing layers of sulphur-very similar to those of CdI_2. The titanium atoms occupy the octahedral holes between the S atoms. Two types of titanium layers alternate along the c axis: filled and partially filled. Actually, in addition to the three basic forms 1T, 4H and 12R, many structures form: 2H, 9R, 8H, 10H...

A superstructure in the $Ti_{1+x}S_2$ was first found by Bartram [19] in the $4H\text{-}Ti_{1.33}S_2$ structure [20]. Some kinds of superstructures designated $(4H)_2$, $(4H)_3$ and $(2H)_2$ were also synthesized and analyzed by means of X-ray diffractometry and high-resolution electron microscopy [20-22].

Each superstructure arises from a specific ordering pattern of Ti vacancies in the partially occupied Ti layers.

A Preliminary observation of diffuse scattering features on the X-ray and electron diffraction patterns on the $Ti_{1+x}S_2$ was made by Moret et al. [23-24]. These diffuse features were attributed to incomplete 2D ordering (Short Range Order SRO or nano-sized domains) of titanium atoms in the partly occupied layers of the structure.

Some metal transition (M) as Fe, Co and Ni, have been successfully inserted into the gap of TiS_2 and show unusual physical properties compared with non-doped/intercalated TiS_2 (see [25-27] and references therein).

In M_xTiS_2 (M = Fe, Ni and Co) several types of superstructures were found (see [28, 29] and references therein) by maximum entropy method, X-ray diffraction and neutron powder diffraction analyses, and are caused by the ordered/partial ordered atomic arrangement of intercalated M atoms.

Recently, many works reported X-ray powder diffraction,electronic, magnetic and thermal properties of M-doped 1T-TiS_2 (M = 3d transition metal). These works have shown that, crystal structure and physical properties of M-doped 1T-TiS_2 depend strongly on the type of guest M atoms, their concentration, and synthesis conditions (see [29,30] and references therein; [31]).

To our knowledge, no germanium intercalated or doped TiS_2 has been reported.

In this study we present our results concerning single crystal X-ray diffraction and transmission electron microscopy, and a study of the metal-metal interactions of the first germanium doped TiS_2 polytypes: 1T, $(4H)_2$, 12R and its corresponding new $a\sqrt{3} \times a\sqrt{3}$ superstructure.

2. Experimental methods

2.1. Synthesis

Single crystals of the title compound were prepared via the CVT (chemical vapor transport) method by two different mixtures of starting materials: pure Ge, Ti and S elements in a ratio 0.5:1:2 and in a mixture of pure Ge and TiS_2 previously prepared in a ratio 0.5:1.

TiS_2 was prepared by heating the appropriate mixture of elements in silica tubes at 900 °C for one week. The tubes were subsequently slowly cooled to room temperature. The mixture was then sealed into an evacuated quartz tube with iodine (<5 mg/cm3) as a transport agent to favour crystallization and heated between 900-1000 °C for 15 days, then slowly cooled to room temperature.

Gray thin platelet-like crystals with rough surface of $M_{1+x}S_2$ (M = Ge/Ti) were obtained with typical lengths between 3 to 7 mm and thickness ranging between 0.02 and 0.07 mm. In addition, some blue crystals of TiO_2 were also obtained in some preparations.

2.2. Single crystal structures description

Four different polytypes were identified in the single crystals of M_xTiS_2 (M = Ge/Ti): 1T, (4H)$_2$, 12R and its corresponding $a\sqrt{3}\ x\ a\sqrt{3}$ superstructure.

The most frequent obtained polytypes are 1T and 12R, and it seems that a mixture of the starting materials with a ratio of 0.5:1 promote the synthesis of polytypes with superstructures as (4H)$_2$ and 12R $a\sqrt{3}\ x\ a\sqrt{3}$. The single crystals of TiO_2 were identified as rutile (tetragonal; a = b = 4.5932(7) Å, c = 2.9656(6) Å; space group P4$_2$/mnm). This is probably caused by both prolonged exposure to air during grinding materials and the affinity of Ti to react with the silica tube at high temperature [32-33].

2.3. X-ray diffraction (XRD)

Single crystals data were recorded on a SMART-APEX CCD X-ray diffractometer (Bruker AXS) with graphite-monochromated Mo Kα radiation.

The reflection intensities were integrated with the SAINT [34]. An empirical absorption correction was applied [35]. Primary structure solution was given by superflip [36], and the structure refinement was performed by Jana 2006 [37].

In the final cycles of refinement, all the atoms in the different structures were refined anisotropically, and the refined occupancy factors (s.o.f) for the sites which did not deviate significantly (about 2%) were reset to full or non occupancy.

Details concerning the structure refinement and final results are presented in Table 1, and atomic coordinates, anisotropic displacement parameters and selected bond distances are listed in Tables S1, S2 and S3 of supporting information.

Supplementary crystallographic data have been deposited via the joint CCDC/FIZ Karlsruhe deposition service. CSD-deposition number 1904551-1904554. These data can be obtained free of charge from FIZ Karlsruhe via www.ccdc.cam.ac.uk/structures.

2.4. Transmission electron microscopy (TEM)

TEM studies were performed on a JEOL JEM 2100 HT microscope equipped with an INCA microanalysis Suite. HRTEM (High Resolution Transmission Electron Microscopy) and HAADF–STEM (High Angle Annular Dark Field- Scanning Transmission Electron Microscopy) images were obtained with a JEOL JEM 3000 F microscope fitted with an

INCA microanalysis Suite. The corresponding single crystals used for X-ray diffraction data were crushed and ultrasonically dispersed in n-butanol, a few drops of the suspension were deposited on a copper grid covered with a holey carbon film as support of the crystallites.

3. Results and discussion

3.1. The 1T-M_1S_2 (M = Ge/Ti)crystal structure

The 1T-$Ti_{1+x}S_2$ is the most stable TiS_2 polymorph which exhibits possible applications in thermoelectric devices. The compound is related to the CdI_2 structure type, and consists of edge-sharing TiS_6 octahedron in a triangular geometry forming S-Ti-S layers and linked to each other by strong covalent interaction within the layers, whereas the layers are linked by weak van der Waals forces. In most cases the self (auto)-intercalation of Ti occurs and the TiS_2 crystals are non-stoichiometric as a consequence of sulphur volatilisation [38-39].

The excess of titanium atoms are located into the van der Waals gap giving the stacking sequence ...aBαCaB...(B, C refer to the sulphur layers; a to the completely filled titanium layers and α to the partially filled titanium layers) (Fig. 1). This non-stoichiometry can affect significantly the thermoelectric properties of the doped/intercalated $Ti_{1+x}S_2$ materials (see [40] and references therein).

The structure of 1T-$M_{\sim 1}S_2$ was refined in the basis of 1T-TiS_2 as host structure. During the refinement, difference Fourier synthesis indicated a maximum peak on the 1b (0 0 ½) position, which was attributed to the excess of titanium (Ti2) with a refined site occupancy about 0.017(2) leading of a decreasing of the residual electronic density.

During the refinement, the mixed occupation of Ti and Ge atoms was checked and it seems almost to occurs in the Ti1 position 1a, with a refined site occupation factor of M (Ge/Ti) = 0.015(6)/0.968(6) i.e., with a total occupation of 98.3% and 1.7% vacancy. Ti1 and Ge1 atoms probably occupied the crystallographic positions 1a in a random fashion. M1-S and M2-S distances (2.4239(5) and 2.4250(5) Å) are close, as observed in other X-ray single crystal structure determinations [41-43, 28].

A characteristic feature of this 1T-structure is the short M1-M2 distance 2.8435(10) Å comparable to the close-contact distance in Ti metal 2.896 Å, this indicates strong metal-metal bonding.

The M atoms are surrounded by 6S + 2M in distorted bicapped octahedrons (CN = 8) linked via one vertex along the c direction (Fig. 1c).

The ionic radius of Ge atoms in a octahedral coordination 0.53Å is smaller than that of Ti atoms 0.604 Å [44], as the Ge atoms replace Ti atoms to form covalent bond, we expect a shrink in the lattice parameters and in the trigonal distortion compared to the host structure. Similar observations were reported in some doped $M_xTi_{1-x}S_2$ [M = Co, Cd, Ni with x = 0.02-0.15, < 0.025, 0.06 respectively) [29, 45, 46 and references therein].

For all atoms, the amplitude of anisotropic displacement parameters (ADP's) U_{33} in the interlayer is larger than the amplitude in-plane U_{11}, indicating weak bonding along the c axis (Fig. 1a). The refinement reveals a strong correlation between the occupation factor of M2 site and its thermal parameters (U_{ij}). Thus it is difficult to refine these two parameters simultaneously; the two Ti atomic positions were then restricted to have the same U_{ij}.

The final refinement converged to reliability factor R_{obs} = 2.48% and R_{wobs} = 2.90%, with the remaining electron densities ($\Delta\rho_{max}$, $\Delta\rho_{min}$) about 0.51 e/Å^{-3} and -0.74 /Å^{-3}.

The composition obtained with the structure refinement is almost stoichiometric 1T-$Ge_{0.015}Ti_{0.985}\square_{0.017}S_2$ i.e., $M_{\sim1}\square_{0.017}S_2$ ($\square$ denotes the vacancies in the M = Ge/Ti positions).

3.2. The 12R-$M_{1.111}S_2$ (M = Ge/Ti) crystal structure

The 12R polytype has been previously studied by different groups [11-12, 19, 47-49]. Its structure was determined by X-ray diffraction [50-51] before the discovery of polytypism in the Ti-S system.

The structure is based on a close packing of sulfur layers with a stacking sequence... BαCbAγ BcAγBaCβAbCβAcBαCa... (A, B, C refer to the sulphur layers; a, b, c to the completely filled titanium layers and α, β, γ to the partly filled titanium layers). The structure can be described by layers of the type prism-prism-octahedron-octahedron [SM$_6$] (Fig. 2).

If we focus on the coordination of the sulfur atoms, there are two types of titanium polyhedrons surrounding an atom of sulfur: trigonal prism or slightly deformed octahedron, different successions of layers of these two types of polyhedrons correspond to the diverse polytypes observed. In the structure 2H, only the first type is present, within 4H both types alternate along the c direction. Every atom of titanium is practically located at the centre of an octahedron of atoms of sulfur.

Unlike to the 1T-doped polytype, the refinement indicate that the mixed occupation of M = Ge/Ti atoms seems to occur in all positions with different occupancy, especially in the partial occupied position, where the occupation factor of Ge range between 3.5-5.7%. The distribution of Ge atoms observed over the fully occupied and partially filled atom layers is 54.76% and 45.23% respectively.

The octahedral holes between adjacent prism-prism and adjacent octahedron-octahedron sulfur layers are not fully occupied by M atoms (the position 3b is refined with 4.8% of vacancy), with six equivalent distances: M-6S = 2.4596(3) Å and 2.4614(3) Å.

The octahedral holes between adjacent prism-octahedron layers are partially occupied by M3 (position 6c). In this case, the refined site occupancy factor is (Ge/Ti) = 0.038/0.109 in a random fashion, with three short M3-S and three long distances 2.3486(16) and 2.5722(19) Å respectively. The $M3S_6$ octahedrons are slightly more distorted (S-M3-S = 83.88(8) – 90.785(11)°) compared to the MS_6 octahedrons (S-M-S = 88.604(11) - 91,395(11)°).

In comparison to the results obtained by Tronc et al. [51], all the atoms are refined anisotropically and there is a slight expansion in the distances and in the c parameter. This expansion is probably caused by the intercalation of Ge atoms, as it was observed in some doped $(M_xTi_{1-x})_{1+y}S_2$ [M = Mn (up to 1), Ni (up to 0.06), and Cu (up to 0.6)] ([52] and references therein; [53, 54]).

The range in the M-S bond distances is due to the corrugation of the M layers as a consequence of M-M pair interactions. In fact, the short M-M distance is about 3.088(3) Å and deviate from the ideal distance 2.896 Å (in Ti metal) as observed in the $4H-Ti_{1.225}S_2$ polytype [55]. This fairly short distance larger by only 0.288 Å than the sum of the atomic radii [56] is still strong enough for M-M bonding interactions.

The M atoms are arranged in 6, 7 and 8 vertex polyhedron (CN= 6, 7 and 8). The coordination polyhedrons of the M1 atoms with two additional M3 are distorted bicapped octahedrons, while the coordination M3 atoms with one additional M1 neighbor are in slightly distorted mono-capped octahedrons; theses polyhedrons are linked via common faces with the distorted octahedrons of M2 along the c direction (Fig. 2c). Higher coordination of titanium atoms was also observed in some titanium rich sulfur Ti_8S_3 and Ti_2S [57, 58].

The amplitude of displacement parameters (ADP's) U_{33} (interlayer) is larger than the amplitude in-plane U_{11} for most atoms except the fully occupied M positions (M1 and M2), in which the thermal motions are nearly isotropic (Fig. 1c). On the other hand, there is no correlation between the occupation factor of M3 site and its ADP's; these two parameters are then simultaneously refined.

The final refinement converged to reliability factor R_{obs} = 2.32% and R_{wobs} = 2.71%, with the remaining electron densities ($\Delta\rho_{max}$, $\Delta\rho_{min}$) about (0.35 e/Å^{-3} and -0.67 /Å^{-3}).

The composition obtained with the structure refinement is 12R-$Ge_{0.084}Ti_{1.027}\square_{0.074}S_2$ i.e., $M_{1.111}\square_{0.074}S_2$, close to that observed by Tronc et al. [51] 12R-$Ti_{1.17}S_2$.

3.3. The $M_{1.206}S_{1.91}$ -12R- $a\sqrt{3}$ x $a\sqrt{3}$ x c superstructure (M = Ge/Ti)

$a_0\sqrt{3}$ x $a_0\sqrt{3}$ superstructures have been observed by different groups [22, 23, 59-61]. They are associated with diverse stacking sequences of the defective layers leading to different 3D-superstructures. All these superstructures arise from ordering of Ti vacancies in the partially occupied Ti layers, being the metal vacancies confined to every second metal layer.

Each polytype has a tendency to generate the corresponding superstructure [61]. The new 2D superstructure $a_0\sqrt{3}$ x $a_0\sqrt{3}$ of 12R $M_{1.1}\square_{0.074}S_2$ polytype was found in our attempt to dope /intercalate germanium into TiS_2 layers. Several single crystals have been tested and the same parameters: a = b = $a_0\sqrt{3}$ = 5.94 Å and c = c_0 = 34.27 Å were obtained (a_0 and c_0 are the parameters of the reference 12R-type structure.

The superstructure is based on a close packing of sulfur of the type prism-prism-octahedron-octahedron [SM_6].

A highly disorder structural model was refined in the P-31m space group (subgroup of the 12R-polytype: R-3m) on the basis of the 12R-polytype, with 10Ti and 8S independent atom sites, obeying to the same stacking sequence aBαCbAγBcAγBaCβAbCβAcBαC (A, B, C refer to the sulphur layers; a, b, c to the completely filled titanium layers and α, β, γ to the partly filled titanium layers) (Fig. 3).

As observed in the 12R-substructure, the mixed occupation of Ge/Ti atoms seems occurs in all positions with different occupancy, in addition to a small number of vacancies in both fully occupied Ti and S layers, probably due to the presence of structural defects. An equal proportion distribution of Ge occupied observed over the fully (54.03%) and partially atoms layers (45.96%) is also observed.

The structure refinement, with statistical replacements of Ti sites by some Ge atoms, exhibit a strong correlation between site occupancies and parameters of thermal motion of such atoms.

The amplitude of displacement parameters (ADP's) in the (ab) plane $U_{11} = U_{22}$ is larger than U_{33} for most atoms; except for partly M positions due to the weaker bonding along the c axis (Fig. 3a).

The refinement was unstable and result in a large parameter U_{33} for M10 position (2/3 1/3 1/2) and significantly the ADP's for M9 position (0 0 1/2), with unrealistic U_{33} value. A stable refinement was obtained by adopting additional disorder in this fully occupied M layer in the form of shifting the 1b M9 atom position to the 2c Wyckoff position (0 0 0.502(3)) and refining the occupancy of the M10 position.

The displacement of M9 atom can be explained by the presence of vacancies at the S2 atom site 6c about 15.6%, which lead to a shift of this atom toward the ideal position.

The refinement converged to rather higher reliability factor $R_{obs} = 13.22\%$ with higher electron densities $\Delta\rho_{max}$ about 5.02 e/Å^{-3} around M10 atom.

A refinement by considering a split- atom model for M9 into two sub-sites with partial occupancy factors failed because of the closeness of the positions and the high correlation generated between all structural parameters of the Ti9/Ge9 atoms especially in the case of position splitting.

The M-S distances range from 2.441(3) to 2.473(3) Å for full occupation atoms positions, and from 2.291(5) to 2.610(5) Å for the distorted M = Ge/Ti atoms in the partial occupation positions.

The M-S distances show more range than those observed in the substructure 12R (2.4596(3)-2.4614(3) and 2.3483(16)-2.5722(19) Å), this range can be explained by the displacement of deficient metallic atomic layers from their ideal positions. These displacements are caused by M = Ge/Ti sublattice distortions, and revealed by structural refinement of some polytype [51, 17].

The four short M-M distances which range from 3.040(4) to 3.068(8) Å are larger by 0.241 to 0.26 Å respectively than the sum of the atomic radii (0.241 to 0.26 Å) [56], and still correspond to strong enough bonding interactions.

As observed in the substructure 12R, the M atoms are then arranged in 6, 7 and 8 vertex polyhedrons (CN = 6, 7 and 8). The coordination of the M atoms within the partly filled layers are slightly distorted mono-capped octahedrons, while the coordination polyhedron of the M atoms within the fully occupied layers alternate between distorted bicapped octahedrons and distorted octahedrons along the c axis (Fig. 3c).

The composition obtained with the structure refinement is $(Ge_{0.11}Ti_{1.096})\square_{0.115}S_{1.91}\Delta_{0.09}$ i.e., $M_{1.206}\square_{0.115}S_{1.91}\Delta_{0.09}$; ($\square$ and Δ denotes the vacancies in the Ti and S positions respectively), taking account of the vacancies the composition is $M_{1.321}S_2$ which is close to the ideal one with x = 0.33 for extra atoms.

However, there are very few polytypic crystals of satisfactory quality; the coexistence of several polytypes together with stacking disorder regions is the most frequent situation.

The X-ray diffraction pattern shows reflections that exhibited a rod-shaped streaking along the c* axis (Supporting information, Fig. 1S). These kinds of diffuse streaks, which have been observed frequently in $Ti_{1+x}S_2$, correspond to a disordered stacking of hexagonal layers and, they hinder conventional structure refinement from X-ray diffraction data.

Diffuse scattering due to the stacking disorder also contributes of the total diffracted intensity. This could explain the rather higher R factor values (13.22%) obtained.

Nevertheless, the results seem to be very reliable in comparison to what has been found for the parent structures in powder diffraction, if we consider the highly disorder, vacancy and some defects which characterize this kind of polytypes.

3.4. The $(4H)_2$-$M_{1.244}S_{1.945}$ superstructure (M = Ge/Ti)

3D-superstructure of 4H-$Ti_{1.33}S_2$ was first found by S.F. Bartram [19]. Two predominant (4H)-based superlattices noted $(4H)_2$-$TiS_{1.46}$ and $(4H)_3$-$TiS_{1.51}$, have been observed and analyzed by means of X-ray diffractometry and high-resolution electron microscopy [20-23, 59 -60].

The 3D-superstructures $(4H)_2$ and $(4H)_3$ are considered to arise from the same type of ordering Ti atoms and vacancies in the partially filled layers, but with different stacking sequences. The stacking sequence lowers the symmetry from $P6_3mc$ in 4H to Cc (subgroup of the 4H-polytype : $P6_3mc$) in both $(4H)_2$ and $(4H)_3$.

In comparison to the earlier study by Onoda et al. [20] in powder diffraction, the superstructure of the current determination was described in the same space group Cc with a measured beta angle about 95° instead 90°, and using only 9M and 12S independent atoms obeying in the (ac) plane to the stacking sequence...AcDγBdCβAcDγBdCβA...(A, B, C refer to the sulphur layers; a, b, c to the completely filled titanium layers and α, β, γ to the partly filled titan-ium layers) (Fig. 4a); there are 3M independent atoms less in the partially filled layers than the model proposed by Onoda et al. [20].

As observed in the 12R-polytype and its superstructure, the mixed occupation of Ge/Ti atoms seems occurs in all positions with different occupancy,in addition to some vacancies in the fully occupied M and S layers.

The refinement indicates a mixed occupation of M = Ge/Ti atoms in all positions with different occupancy, especially in the partially occupied position, the occupation factor of Ge

range between 3.5-5.7%. On the other hand, there is no correlation between site occupancies and parameters of thermal motion of such atoms, these two parameters are refined simultaneously.

The proportion of the distribution of Ge atoms over the fully (52.50%) and partially occupied atom layers (47.50%), is comparable to the proportion observed in the two 12R-polytypes.

In comparison, with other polytypes, all the M atoms are surrounded by six different sulphur atoms. The M-S distances range from 2.365(16) to 2.540(7) Å for full occupation positions, (correspond to M6) and from 2.293(8) to 2.587(18) Å for partial occupation positions (correspond to M8).

The range observed in M-S distances is more significantly than observed in other polytypes, and we can expect more distortions of metallic atomic layers from their ideal positions. The three short M-M distances range from 3.034(7) to 3.144(5) Å, are larger by 0.234 to 0.344 Å respectively than the sum of the atomic radii, and still correspond to strong enough M-M bonding interactions.

As observed in the sub-structure 4H-$Ti_{1.225}S_2$ [54], the M atoms are arranged in 6 and 7 vertex polyhedrons (CN = 6 and 7). The coordination of M atoms within the partly filled layers are slightly distorted mono-capped octahedrons, while the coordination polyhedron of the M atoms within the fully layers are distorted mono-capped octahedrons or distorted octahedrons along the c axis (Fig. 4c).

The amplitude of displacement parameters (ADP's) in the (ab) plane U_{11} and U_{22} is larger than U_{33} for most atoms include the partly M positions. This suggests that these atoms are shifted toward their positions, and the M polyhedrons are likely to tilt each other within the (ab) plane. Such ADP's for the M atoms in the partially occupied position is common for some intercalate compounds in TiS_2 [62, 28], the less amplitude of U_{33} can be explained by the large occupancy factors (s.o.f) between 0.478 and 0.728, the M atoms are then less disordered com-pared to the 12R-superstructure or other polytypes.

The final refinement converged to reliability factor R_{obs} = 5.20% and R_{wobs} = 10.29%, with the remaining electron densities ($\Delta\rho_{max}$, $\Delta\rho_{min}$) about (0.75 e/Å^{-3} and -0.60 /Å^{-3}).

The composition obtained with the structure refinement is $(Ge_{0.04}Ti_{1.204})\square_{0.044}S_{1.945}\Delta_{0.55}$ i.e., $M_{1.244}\square_{0.044}S_{1.945}\Delta_{0.55}$ is less by 6.57% of M atoms than the composition obtained by Onoda et al. [20] with $M_{1.37}S_2$. Taking account of vacancy the composition obtained is about $M_{1.288}S_2$, which is almost close the ideal one with x = 0.33 for extra atoms.

3.5. The Metal -Metal interactions (M= Ge/Ti)

In the TiS_2 system, linkage of octahedra by face sharing gives short metal-metal distance. This M-M pair interaction indicates strong metal-metal bonding, but can also be analyzed in terms of electrostatic repulsion.

The current crystal structures refinement of the different polytypes support the conclusions reported in references [63, 60].

The results show that the atoms are shifted away from the center of octahedron, as a consequence of metal-metal M-M corrugated layers across the sulfur layers (Supporting information, Fig. 2S).

The M-S distances are then altered with short and long distances, especially in the metal partially occupied layers.

The distortion $\delta(Å)$ observed in the M-S distances, which expressed the difference between the longest and the shortest distances is more significant in the superstructures compared to the correspondent basic-structure (Fig. 5a). Within the same superstructure polytype, this distortion seems altered or decreases with M-M distances but in a non-linear way. The larger value of distortion is observed in the 12R superstructure at the M8 atom, and it can be explained by the presence of vacancies at the S atoms (ranging from 8.1% to 15.6%), which lead to a shift of the M atom towards the ideal position (Supporting information , Fig. 3Sa).

The fact that the M-M distances deviate from the ideal values, is a very common feature of TiS_2 polytypes, but the frequency of occurrence of short M-M distances and their deviations from the ideal value are more significantly within long-range ordering of M atoms in 2D (12R) or in 3D $(4H)_2$ superstructures (Fig. 5b).

An increase of M-M distances within the same superstructure polytypes is observed along with the varying increasing of the site occupation factor (s.o.f) of M atoms in the partially filled layers, probably in order to minimize the M-M electrostatic repulsions, but this tendency don't exhibit a linear behavior (Supporting information, Fig. 3Sb).

A mixed occupation of Ge/Ti atoms with different occupancy distributed over most of the M sites is obtained during the current refinements. Except in the 1T-polytype, an almost equal proportion of the distribution of Ge atoms is observed over the fully and partially occupied layers, with the increasing concentration of the Ge atoms in the polytype. Indeed, a strong replacement of Ti atoms in the partially layers by Ge atoms would destabilize the structure by breaking the Ti-Ti interactions across the face-sharing octahedral, the Ge atoms have to occupy some sites in the fully layers. A similar phenomenon was observed in some non-stoichiometric chromium titanium selenides [64].

Except the 1T-polytype, both the short (*s*) and the long (*l*) M-M distances alternate on parallel zigzag chains along the c direction in the sequence *s-l-s-l* for 4H and *s-s-l-l-s-s* for 12R; 12R-sperstructure and $(4H)_2$ polytypes (Supporting information, Fig. 4S). The shortest M-M distance 2.8435(10) Å is observed in the most stable polytype $1T-M_{\sim 1}\square_{0.017}S_2$, with a low s.o.f of M atoms in the partially filled layer; shorter M-M distances should correspond to decreased repulsions and longer distances to increased repulsion. The relaxation probably occurs following a defect model by introducing vacancy in the adjacent M filled layer, the atoms are then displaced toward the created vacancy to minimize the formation of M-M pairs interaction Tronc and Moret [60, 65]; this can explain the observation of some vacancy in the filled M layers during the different structures refinement by X-ray diffraction.

This 2D and 3D ordering superstructures, seems to affect also the amplitude of displacement parameters (ADP's) in the (ab) plane, U_{11} and U_{22} become larger than U_{33} for most atoms including the partially M positions as observed in the $(4H)_2$-superstructure.

The Bond-valence model was used to calculate the Bond-valence-sum BVS of M atoms, using the M-S results obtained for the four polytypes [66] range from 3.275 to 3.887 v.u. (Supporting information, Table S4).

The higher BVS values are observed for M atoms in the partially filled layers and are almost close to their formal valence state +4, while the BVS for M atoms in the filled layers are lower. This trend can be explained by a valence compensated between the M atoms in order to keep the number of electrons transferred to the S atoms roughly constant.

Additionally, a correlation exists between the calculated valence of M atoms and the M-M distances. M atoms which BVS decreases with increasing of M-M distances, seems occur in pairs between adjacent M layers.

This correlation can be correspondingly interpreted as a valence ordering of M atoms, caused by an adjustment of the M-M distances in order to minimize the electrostatic repulsion.

This kind of complex pattern with changes of M-M distances and valences was also observed in some Magnéli phases [67].

3.6. Electron Microscopy

The analysis results by X-ray energy dispersive spectroscopy (XEDS) with the TEM, summarized in Table 2, are the average of 3 to 5 measurements on several different crystallites of each polytype sample, which yields to a composition $M_{1+x}S_2$ (M = Ge/Ti) in the range 1.02 < 1+x < 1.40.

The XEDS spectrum in Fig. 6 shows the simultaneous presence of Ge, Ti and S elements. The Ge energy peaks were clearly identified at 2.1 Kev ($L\beta_1$) and 9.8 Kev ($K\alpha$) respectively. The highest Ge-doping level was observed in the monoclinic sample with 7.08% atomic ratio.

Fig. 7a shows a SAED (Selected Area Electron Diffraction) pattern of $1T$-$M_{1+x}S_2$ (M = Ge/Ti , x ~ 0.05) taken along *[0001]* zone axis, only the basic reflections of $1T$-TiS_2 are observed.

The SAED patterns shown in Figs. 7b-d correspond to a $12R$-TiS_2 polytype structure. In addition to the strong basic reflections, a highly structured diffuse scattering surrounding the main spots is observed, which is similar to that observed in $Ti_{1+x}S_2$ [23, 24, 68, 69] and in some of the intercalate compounds A_xNbX_2 (A = Ge, Fe and X= S, Se) [70, 71]. It can be attributed to the short-range ordering of M = Ge/Ti atoms in the partially-filled layers. These diffuse segments are arranged in triangles sharing vertices, and they correspond to $2a^*$ x$2a^*$ superstructure. The Fig. 7d, with x ~ 0.40, shows an increase of the length and the intensity of these diffuse segments accompanying the main reflections. In addition to the main reflections and structured diffuse scattering, sharp weak spots are also observed in the position of the forbidden *10-10* type reflections of Figs. 8b-d, they correspond to the intercepts of streaking running along c* (see Fig. 8b). Isolated stacking faults may account for the aforementioned streaking running among main reflections.

Fig. 8a shows the HRTEM image with x ~ 0.21 taken with the incident beam parallel to the stacking direction *[0001],* note the mottled contrast associated to the SRO.

The SAED patterns shown in Figs. 8b and 8e, with x ~ 0.21 are characteristic of the $12R$-$M_{1+x}S_2$ polytype; the lattice spacing measured along *00l* reflections is 1.16 nm, which did not vary from one pattern to another and it corresponds to one third of the *c* axis, as it was observed by R.J.D. Tilley [47] for the composition $Ti_{1.25}S_2$.

The lattice parameters measured in the SAED patterns (Fig. 8b) are a = 0.30 nm and c = 3.45 nm (1.15 x 3 nm), in good agreement with the lattice parameter of the host structure measured by X-ray diffraction (a = 0. 34 nm and c = 3.46 nm).

Figs. 8c and 8d show the HRTEM and HAADF-STEM images taken along the *[2-1-10]* zone axis, with a 12R stacking sequence …AγBCαBCβA…

The fact that the $2a^*$ x $2a^*$ superstructure is revealed only by electron diffraction, suggest the presence of microdomain with different ordering schemes of extra atoms M, too small to be observed by X-ray diffraction (see Fig. 8f).

The $12R$-$a\sqrt{3}$ x $a\sqrt{3}$ superstructure is revealed by both, electron diffraction and X-ray diffraction by the presence of satellite reflections. Fig. 9a is a SAED pattern of a $12R$-$M_{1+x}S_2$ crystal flake taken along the *[0001]* zone axis, the pattern consist of the strong basic

reflections of the rhombohedral polytype and additional weaker satellite reflections located at *1/3 <11-20>**. Figs 9b and 9c show a *[2-1-10]* zone axis SAED pattern and the corresponding HRTEM image, where a 12R stacking sequence… AγBCαBCβA…is evidenced. Fig. 9d show a *[1-100]* zone axis SAED pattern, in addition to the strong basic reflections, rows of diffuse intensity along $c^*$are observed and marked by arrows, these rows intercept at 1/3 and 2/3 of *[11-20]** and they are assigned to the ordering of extra atoms and vacancies. In the corresponding HRTEM image (Fig. 9e) the arrows highlight this threefold order along *[11-20]**, i.e. √3a; notice the disorder along the stacking direction c^*, which give rise to the diffuse intensity rows along c^*.

References

[1] J. A. Wilson, A. D. Yoffe, Adv. Phys. 18 (1969) 193-335.

[2] A. D. Yoffe, Annu. Rev. Mater. Sci. 3 (1973) 147-170.

[3] A. Yoon, Z. Lee, Appl. Microsc. 47 (2017) 19-28.

[4] S. Manzeli, D. Ovchinnikov, D. Pasquier, O. V. Yazyev and A. Kis, Nature. Reviews. Materials. 2 (2017) 17033.

[5] A. A. Tedstone, D. J. Lewis, P. O'Brien, Chem. Mater. 28 (2016) 1965−1974.

[6] A. Kuc, T. Heine, A. Kis, MRS Bull. 40 (2015) 577-584.

[7] W. Choi, N. Choudhary, G. H. Han, J. Park, D. Akinwande and Y. H. Lee, Mater. Today. 20 (2017) 116-130.

[8] A. H.Thompson, F. R.Gamble, C. R. Symon, Mater. Res. Bull. 10 (1975) 915−919.

[9] M.S. Whittingham, Prog. Solid State Chem. 12 (1978) 41-99.

[10] M. S. Whittingham, Science. 192 (1976) 1126−1127.

[11] Y. Jeannin, Ann. Chim. 7 (1962) 57.

[12] J. J. Legendre, R. Moret, E. Tronc and M. Huber, Prog. Cryst. Growth Charact. Mater 7 (1983) 309-342

[13] J. Chen, S.-L. Li, Z.-L. Tao, F. Gao, Chem. Commun. 8 (2003) 980-981

[14] M. Nath, C.N.R. Rao, Angew. Chem. Int. Ed. 41 (2002) 3451-3454.

[15] A. Margolin, R. Popovitz-Biro, A. Albu-Yaron, L. Rapoport, R. Tenne, Chem. Phys. Lett 411 (2005) 162-166.

[16] J. L. Murray, Bull. Alloy Phase Diagr. 7 (1986).

[17] J. J. Legendre, R. Moret, E. Tronc, and M. Huber, J. Appl. Crystallogr. 8 (1975) 603-608

[18] E. Tronc, M. Huber, J. Phys. Chem. Solids. 34 (1973) 2045-2058.

[19] S. F. Bartram, Dissertation Abstracts,. 19 (1958) 1216-1216.

[20] M. Onoda, M. Saeki, I. Kawada, Z. Anorg. Allg. Chem. 457 (1979) 62-74.

[21] Y. Bando, M. Saeki, Y. Sekikawa, Y. Matsui, S. Horiuchi, M. Nakahira, Acta Crystallogr 35 (1979) 564-569.

[22] Y. Bando, M. Saeki, M. Onoda, I. Kawada and M. Nakahira, J. Solid State Chem. 34 (1980) 381-384.

[23] R. Moret, M. Huber, R. Comès, Phys. Status Solidi. (a) 38 (1976) 695-700.

[24] R. Moret, M. Huber, R. Comès, J. Phys. Colloques. 38 (1977) C7-202-207.

[25] K. Suzuki, O. Nakamura, T. Kondo, T. Enoki, J. Phys. Chem. Solids. 57 (1996) 1133-1136.

[26] T. Matsushita, S. Suga, A. Kimura, H. Negishi, M. Inoue, Phys. Rev. B60 (1999) 1678.

[27] A. A. Titov, E. G. Shkvarina, A. I. Merentsov, A. A. Doroshek, A. S. Shkvarina, Yu. M. Zhukovc, A. G. Rybkinc, S. V. Pryanichnikov, S. A. Uporov, A. N. Titov. J. Alloys. Compd. 750 (2018) 42-54.

[28] T. Kawasak, K. Ohshima, J. Phys. Soc. Jpn. 80 (2011) 044601.

[29] G. Guélou, P. Vaqueiro, J. Prado-Gonjal, T. Barbier, S. Hébert, E. Guilmeau, W. Kockelmann, A. V. Powell, J. Mater. Chem. C. 4 (2016) 1871-1880.

[30] J. Zhang, X.Y. Qin, H.X. Xin, D. Li, C.J. Song, J. Electron. Mater. 40 (2011) 980-986.

[31] M. Beaumale, T. Barbier, Y. Bréard, B. Raveau, Y. Kinemuchi, R. Funahashi, E. Guilmeau, J. Electron. Mater. 43 (2014) 1590–1596.

[32] M. Beaumale, T. Barbier, Y. Bréard, G. Guelou, A. V. Powell, P. Vaqueiro, E. Guilmeau Acta Mater. 78 (2014) 86–92.

[33] Y. Arnaud, M. Chevreton, J. Solid State Chem. 9 (1974) 54-62.

[34] SAINT 6.28A, Bruker AXS Inc. Madison, 1997–2001.

[35] G.M. Sheldrick, SADADS v. 2.03 Bruker AXS Inc., Madison, 1997–2001. Sheldrick, G. M. (2002). SADABS. University of Gottingen, Allemagne.

[36] L. Palatinus, G. Chapuis, J. Appl. Crystallogr. 40 (2007) 786–790.

[37] V. Petříček, M. Dušek, JANA2006, Structure Determination Software Programs, Institute of Physics, Praha, Czech Republic, 2006.

[38] J. C. Mikkelsen, Il Nuovo Cim. B38 (1977) 378–386.

[39] J. Bernard, Y. Jeannin, Adv. Chem. 39 (1963) 191-203.

[40] M. Zhang, C. Zhang, Y. You, H. Xie, H. Chi, Y. Sun, W. Liu, X. Su, Y. Yan, X. Tang, C. Uher, ACS Appl. Mater. Interfaces. 10, 38 (2018) 32344-32354.

[41] *C*. Riekel*, R*. Schöllhorn, Mater. Res. Bull. 10 (1975) 629-634.

[42] R.E. Nikolaev, D.A. Piryazev, A.V. Virovets, N.G. Naumov, Inorg. Mater. 52 (2016) 13–18.

[43] E. Tronc, R. Moret, Synth. Met. 4 (1981) 113-118.

[44] R.D. Shannon, Acta Crystallogr. A32 (1976) 751-767.

[45] J. Zhang, X.Y. Qin, D. Li, H.X. Xin, L. Pan, and K.X. Zhang, J. Alloys Compd. 479 (2009) 816-820.

[46] J. Zhang, X.Y. Qin, H. X. Xin, D. Li, C. J. Song, J. Electron. Mater. 40 (2011) 980-986.

[47] R. J. D. Tilley, J. Solid State Chem. 7 (1973) 213-221.

[48] M. Saeki, M. Onoda, Bull. Chem. Soc. Jpn. 55 (1982) 113-116.

[49] M. Saeki and M. Onoda, *Bull. Chem. Soc. Jpn.* 55 (1982) 3144-3146.

[50] E. Flink, G. A. Wiegers, F. Jellinek, Recl. Trav. Chim. Pays-bas. 85 (1966) 869-872.

[51] E. Tronc, R. Moret, J.J. Legendre, M. Huber, Acta Crystallogr. B31 (1975) 2800-2804.

[52] M. Inoue , H. P. Hughes, A. D. Yoffe, Adv. Phys. 38 (1989) 565-604.

[53] J. Zhang, X.Y. Qin, D. Li, H.Z. Dong, J. Phys. D: Appl. Phys. 39 (2006) 1230-1236.

[54] T. Kusawake, Y. Takahashi, K. Ohshima, Mater. Res. Bull. 33 (1998) 1009-1014.

[55] L.J. Norrby, H.F. Franzen, J. Solid State Chem. 2 (1970) 36-41.

[56] J.C. Slater, J. Chem. Phys. 41 (1964) 3199–3204.

[57] J.P. Owens, H.F. Franz, Acta Crystallogr. B30 (1974) 427-430.

[58] J.P. Owens, B. R. Conrad, N. F. Franzen, Acta Crystallogr. 23 (1967) 77-82

[59] R. Moret, E. Tronc, Y. Bando, M. Saeki, Y. Sekikawa, Y.Matsui, S. Horiuchi, M. Nakahira, Acta Crystallogr. B36 (1980) 2854-2855.

[60] E. Tronc, R. Moret, J. Solid State Chem. 36 (1981) 97-106.

[61] M. *Onoda,* M. Saeki, Acta Crystallogr. B39 (1983*)* 34-39*.*

[62] T. Kawasaki, K. Ohshima, J. Phys. Soc. Jpn. 77 (2008) 054601.

[63] G.A. Wiegers, F. Jellinek, J. Solid State Chem. 1 (1970) 519-525.

[64] J. Wontcheu, W. Kockelmann, Z.L. Huang, W. Schnelle, W. Bensch, Solid State Sci. 9 (2007) 506-514.

[65] E. Amzallag, I. Baraille, H. Martinez, M. Rérat, M. Loudet, D. Gonbeau, J. Chem. Phys. 127 (2007) 074703-8.

[66] (a) I. D. Brown, D. Altermatt, Acta Crystallogr. B41 (1985) 244–247.

(b) N. E. Brese, M. O'Keeffe, Acta Crystallogr. B47 (1991) 192–197.

(c) C. Hormillosa, S. Healy, T. Stephen, I. D. Brown, Bond Valence Calculator. (1993) McMaster University, Canada. http://CCP14.ac.uk   and http://www.CCP14.ac.uk/solution/ bond_valence/.

[67] Y. Le Page, P. Strobel, J. Solid State Chem. 47 (1983) 6-15.

[68] R. de Ridder, Physica B+C. 99 (1980) 39-46.

[69] K.S. Bartwal, Philosophical Magazine B. 71 (1995) 895-901.

[70] M. Kars, A. Gomez-Herrero, A. Rebbah , L. C. Otero-Diaz, Mater. Res. Bull. 44 (2009) 1601–1607.

[71] G. Van Tendeloo, R. De Ridder, L. Van Goethem, P. Van Dyck, J. Van Landyt, S. Amelincks, Phys. Status Solidi A 42 (1977) 319-335.

Table 1

Selected single crystal data and structure refinement parameters for the $1T$-MS_2, $12R$-$M_{1.111}S_2$, $12R$-super $M_{1.206}S_{1.91}$, $(4H)_2$-$M_{1.244}S_{1.945}$ (M = Ge/Ti) polytypes.

$M_{1+x}S_2$ Polytype	$1T$-M_1S_2	$12R$-$M_{1.111}S_2$	$12R$-super$M_{1.206}S_{1.91}$	$(4H)_2$-$M_{1.244}S_{1.945}$
Molar mass (g.mol^{-1})	112.4	119.4	121.6	122.9
Crystal size (mm^3)	0.22 x 0.12 x 0.02	0.41x 0.35 x 0.02	0.16 x 0.11 x 0.10	0.25 x 0.16 x 0.07
Space group	P-3m1	R-3m	P-31m	Cc
Z	1	6	18	24
Unit cell dimensions (Å)	a = 3.4014(6)	a = 3.4383(13)	a = 5.9424(5)	a = 5.97(3)
	c = 5.687(10)	c = 34.590(13)	c = 34.276(3)	b = 10.339(5)
				c = 23.0249(10)
				β = 94.980(9)
Volume (Å^3)	56.981(17)	356.2(2)	1048.20(15)	1415 (6)
Calculated density (g.cm^{-3})	3.2737	3.339	3.467	3.4603
Absorption coefficient (mm^{-1})	5.277	6.054	6.627	6.055
Angular range T (º)	6.93- 27.26	3.51-28.63	1.19 - 40.28	1.78-28.67
Index ranges	-4< h <3 / -4< k <3	-3< h<4 / -4< k<4	-8< h<10 / -8< k<6	-7< h <5 / -13< k<13
	-7< l <7	-45<l<35	-61<l<62	-30< l <30
Rint	0.0353	0.0675	0.0432	0.0337
Total recorded reflections	381	1036	39861	6280
Independent reflections	66 (Rint =0.0353)	150 (Rint =0.0675)	2467 (Rint =0.0432)	2647 (Rint =0.0432)
Reflections with I> 3σ(I)	66	146	1800	1188
T_{min}/T_{max}	0.707/0.902	0.4624/0.7833	0.2769/0.5148	0.3877/0.6547
Data	10	19	77	204

Goodness-of-fit on F^2	1.98	1.93	2.86	1.15
$(R/R_w)_{obs}$ (%)	0.0248/ 0.0290	0.0232/ 0.0271	0.1322/ 0.0923	0.0519/ 0.1027
$(R/R_w)_{all}$ (%)	0.0248/ 0.0290	0.0234/ 0.0271	0.1681/ 0.1042	0.1347/ 0.1174
$\Delta\rho_{max}$, $\Delta\rho_{min}$ (e$^-$/Å^3)	0.51, -0.74	0.35, -0.67	5.03, -3.04	0.72, -0.61

Table 2.

XEDS results obtained from different crystallites of each polytype $M_{1+x}S_2$ (M = Ge/Ti) sample.

$M_{1+x}S_2$ polytype	Ge (at.%)	Ti (at.%)	S (at.%)	$1+x$ = M/S
1T	0.41-1.79	33.92-34.46	63.82-65.45	1.05-1.10
12R	0.14-0.54	37.22-40.90	58.78-62.39	1.21-1.40
12R-super	0.9-3.7	38.86-37.87	62.10-61.09	1.22-1.27
(4H)$_2$	0.23-7.08	33.91-35.97	56.52-70.10	1.02-1.40

Figure Captions
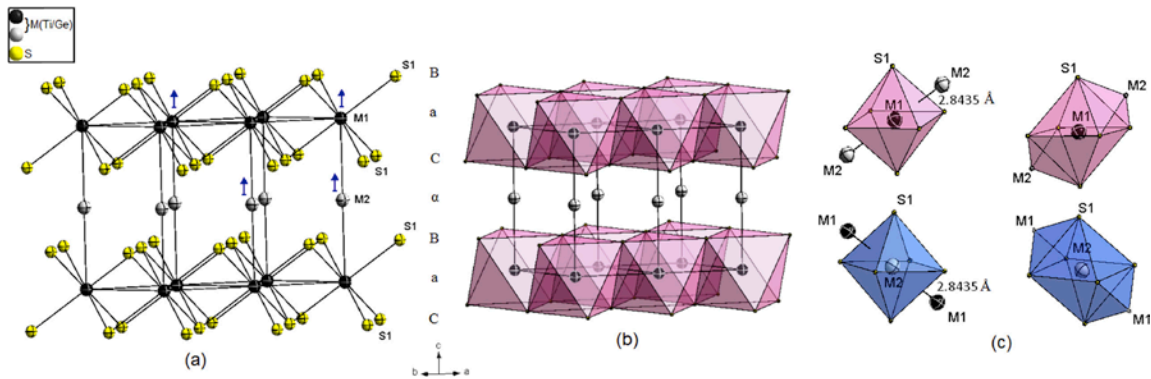
Fig. 1. Crystal structure of 1T-MS$_2$ (M = Ge/Ti). (a) Trigonal prismatic packing of sulphur layers. (b) Clinographic view of the edge sharing MS$_6$ octahedrons. (c) Distorted bicapped octahedral coordination around metal atoms, showing the short M-M distance.

Colour key: Metal atoms (M) in the fully and partially layers are drawn as black and grey respectively, including 95% probability displacement ellipsoids. The blue arrow indicates the dominant thermal vibration direction of M atoms (ADP's). Polyhedron around metal atoms in the fully and in the partially layers are drawn in pink and blue respectively.
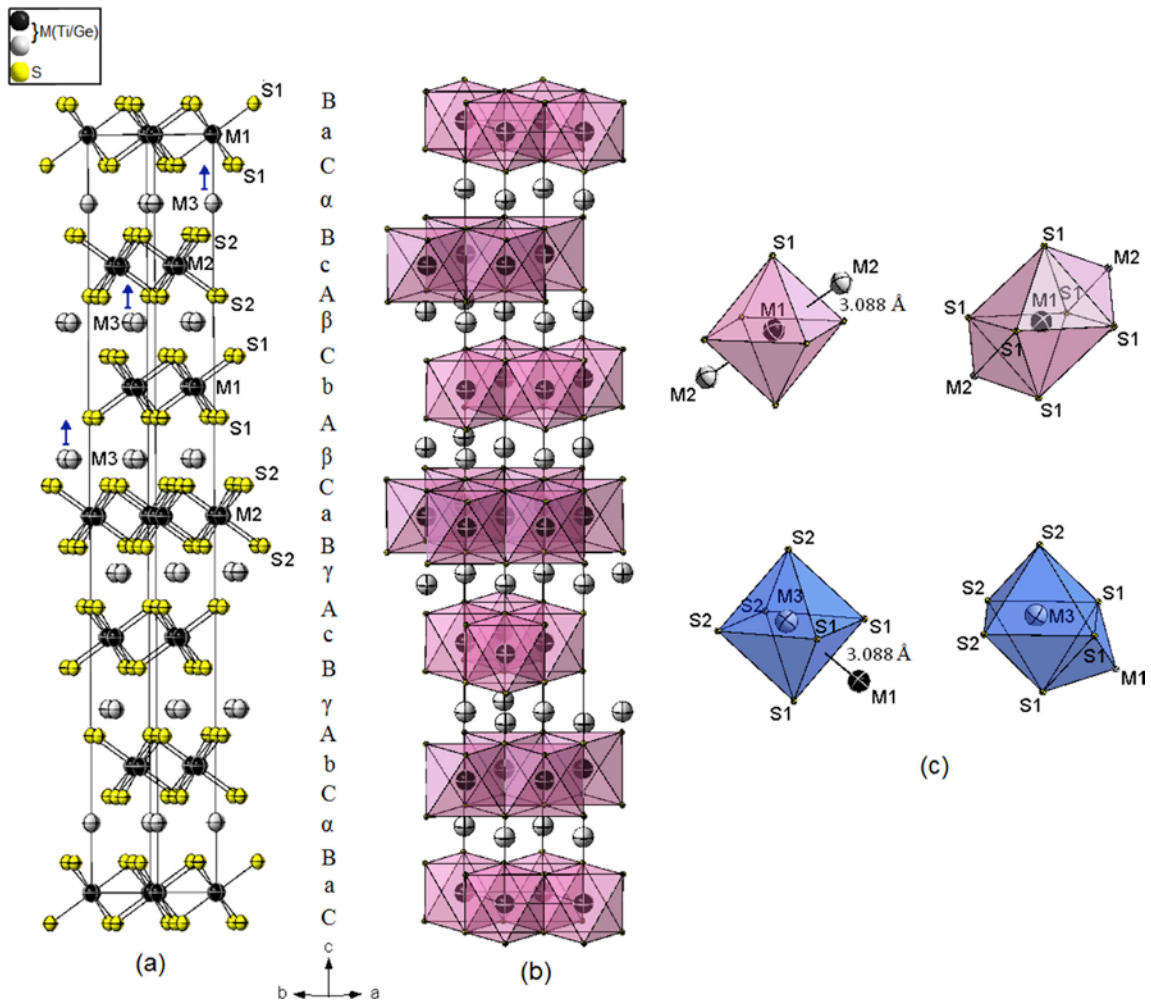
Fig. 2. Crystal structure of 12R-$M_{1.111}S_2$ (M = Ge/Ti). (a) Prism -prism-octahedron-octahedronpacking of sulphur layers. (b) Clinographic view of the edge sharing MS_6 octahedrons. (c) Distorted bicapped and monocapped octahedral coordination around metal atoms showing the short M-M distances. The colour key is as in Fig. 1.
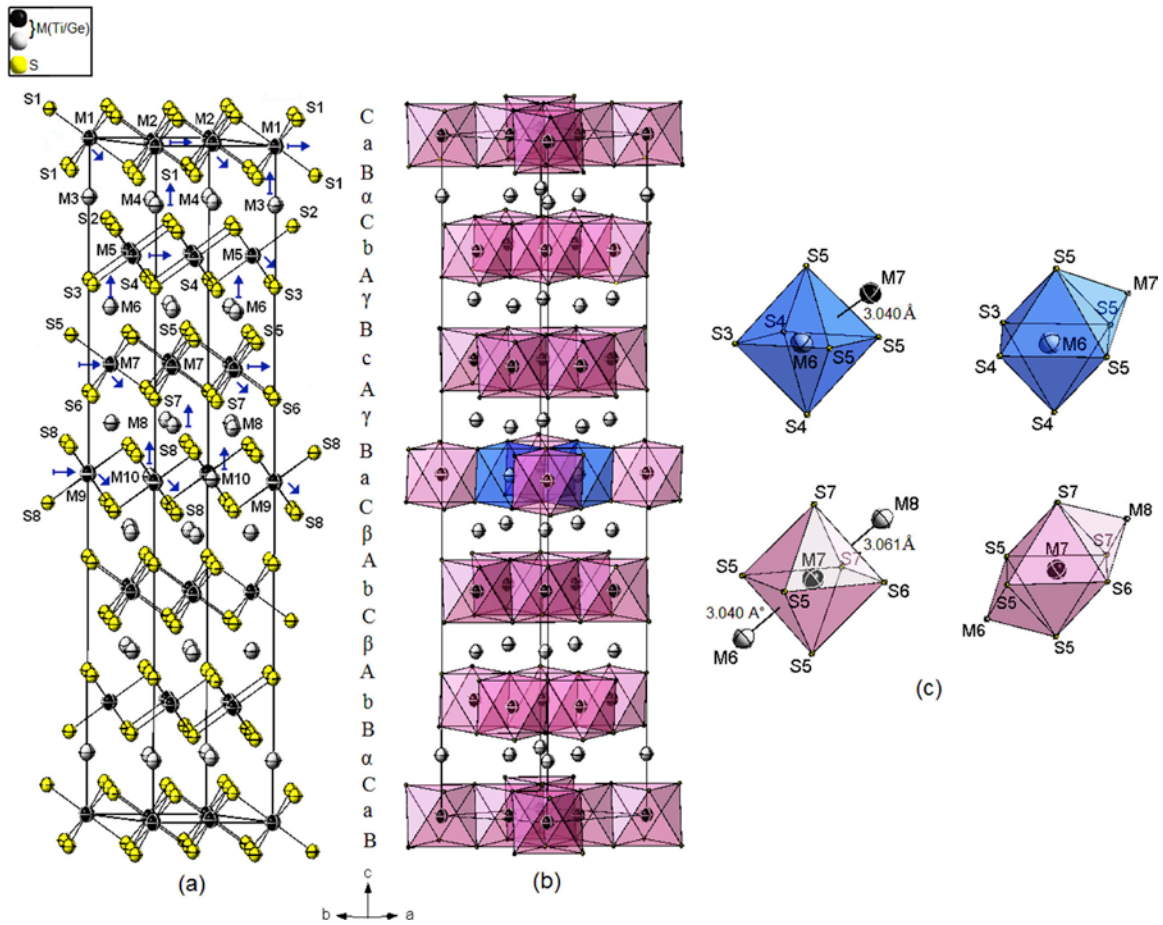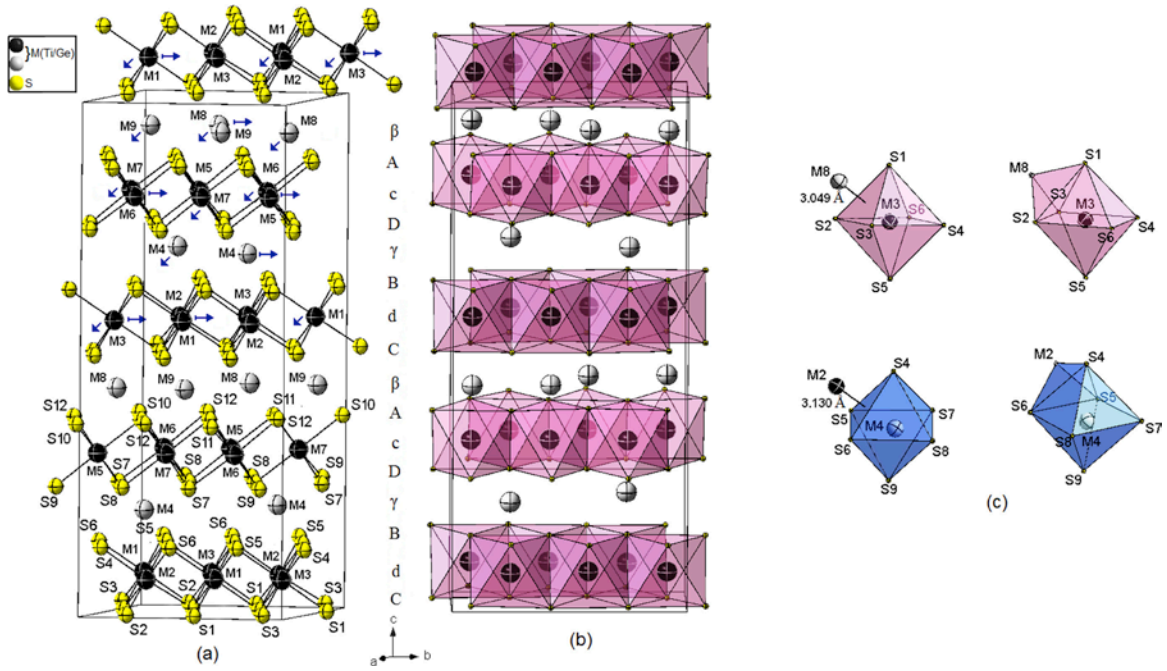
Fig. 3. Crystal structure of 12R-super $M_{1.206}S_{1.91}$ (M = Ge/Ti). (a) Prism-prism-octahedron-octahedron packing of sulphur layers. (b) Clinographic view of the edge sharing MS_6 octahedrons. (c) Distorted bicapped and monocapped octahedral coordination around metal atoms showing the short M-M distances. The colour key is as in Fig. 1.

Fig. 4. Crystal structure of $(4H)_2$-$M_{1.244}S_{1.945}$ (M = Ge/Ti) superstructure. (a) Prism- -octahedron- prism –octahedron packing of sulphur layers. (b) Clinographic view of the edge sharing MS_6 octahedrons. (c) Distorted monocapped octahedral coordin-ation around metal atoms showing the short M-M distances. The colour key is as in Fig. 1.
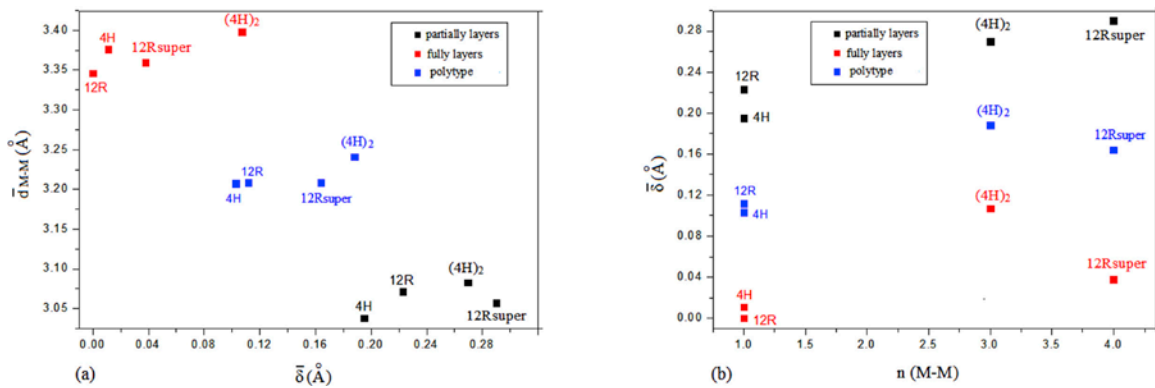
Fig. 5. (a) Variation of the mean distortions $\bar{\delta}$(Å) with the mean of the short distances $\bar{d}$ (M-M) (Å) in the 4H-$M_{1.225}S_2$ [55], 12R-$M_{1.111}S_2$, 12R-super $M_{1.206}S_{1.91}$ and the $(4H)_2$-$M_{1.244}S_{1.945}$ (M = Ge/Ti) polytypes. (b) Variation of the mean distortions $\bar{\delta}$(Å) with frequency observation of short distances n (M-M) in the 4H-$M_{1.225}S_2$ [55], 12R-$M_{1.111}S_2$, 12R-super $M_{1.206}S_{1.91}$ and the $(4H)_2$-$M_{1.244}S_{1.945}$ (M = Ge/Ti) polytypes.

Element	Weight%	Atomic%
S K	44.53	56.52
Ti K	42.85	36.40
Ge K	12.63	7.08
Totals	100.00	100.00
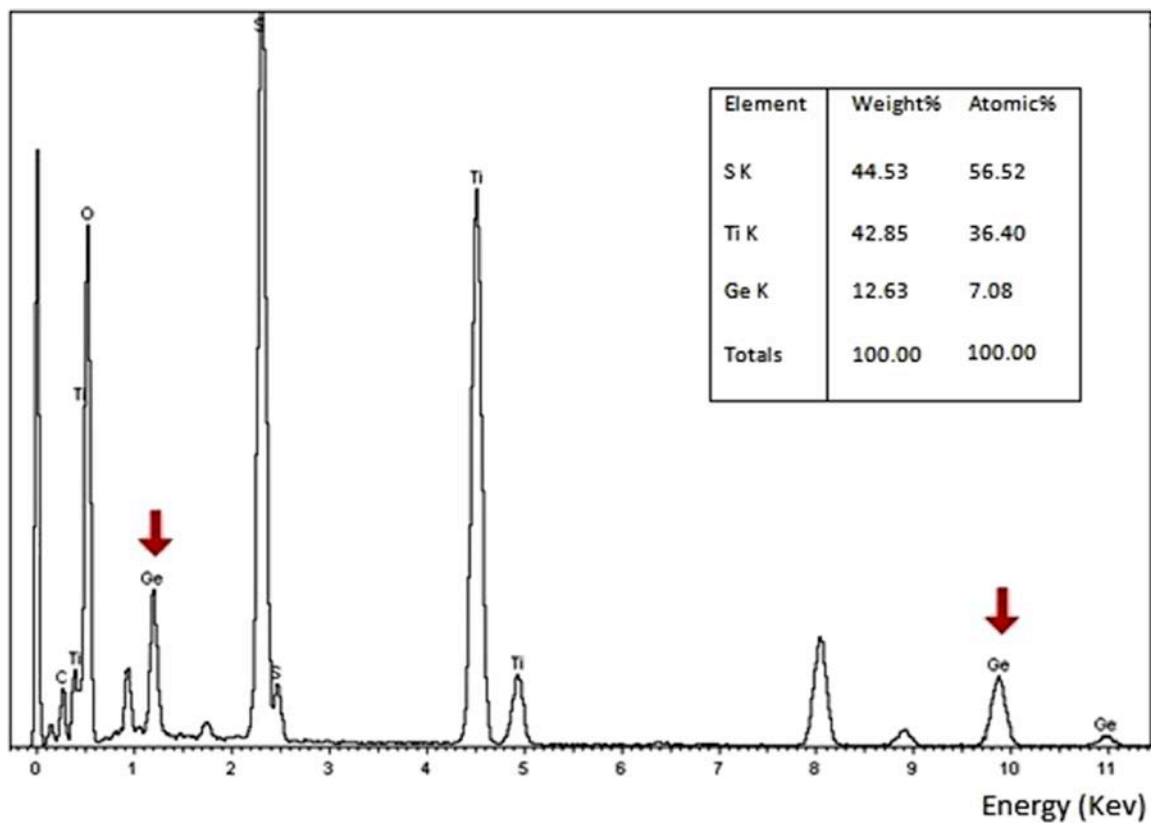
Fig. 6. Typical TEM-EDS spectra obtained on single crystals of the monoclinic sample, showing the presence of Ge energy peaks at 2.1 Kev (Lβ_1) and 9.8 Kev (Kα) respectively.
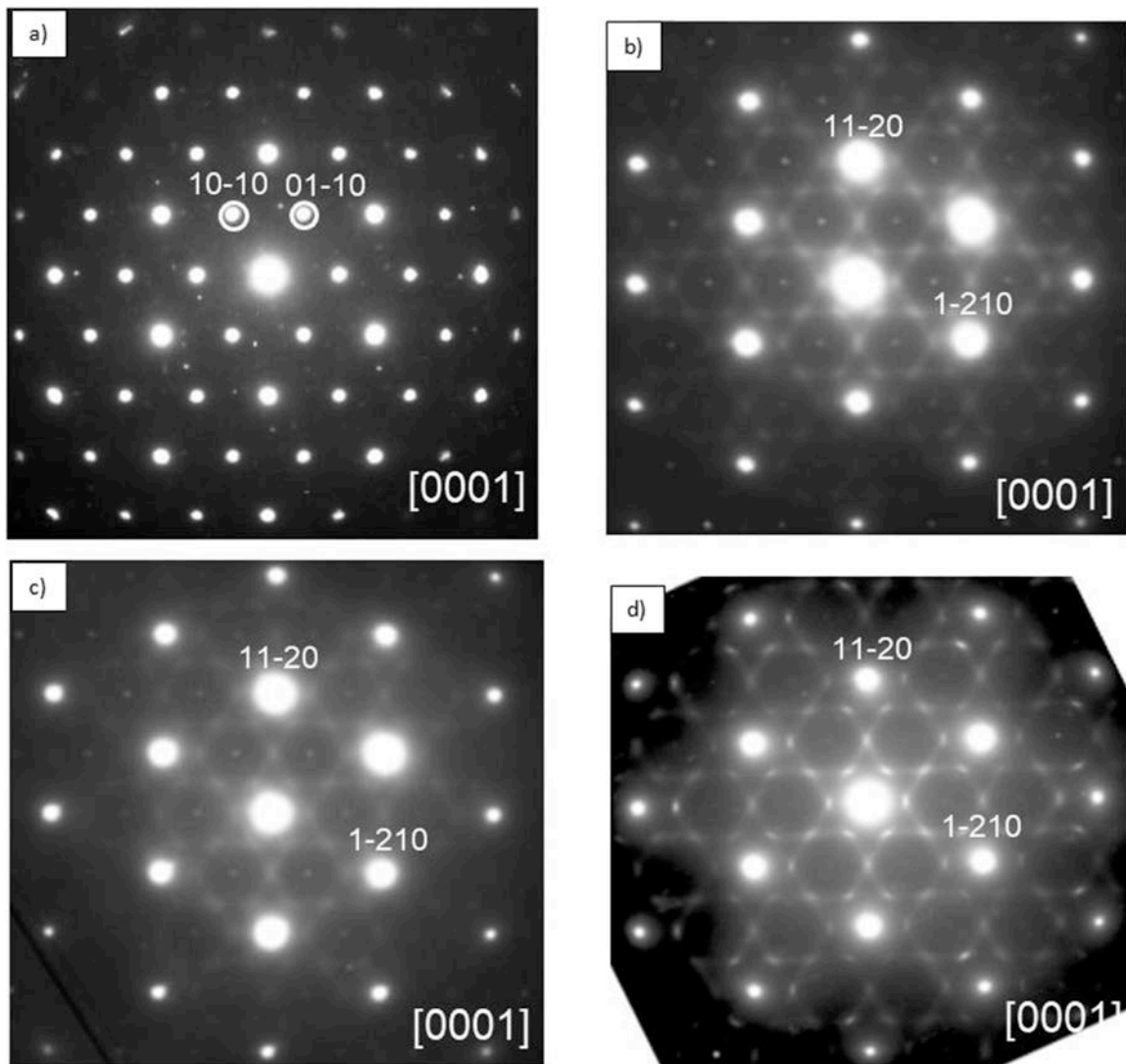
Fig. 7. (a) *[0001]* zone axis SAED patternof 1T-$M_{1+x}S_2$ (M = Ge/Ti), for x ~ 0.05, only the basic reflections are observed. (b, c) for x ~ 0.23 and x ~ 0.25 (M = Ge/Ti), the pattern consist of the basic reflections of 12R-$M_{1+x}S_2$ and a structured diffuse scattering distribution made up of curved segments arranged in triangles sharing vertices, sharp weak spots with periodicities *a* x b** (a is the parameter of the-basic unit cell) are also observed and marked with arrows. (d) for x ~ 0.40, the SAED pattern showan increase of the length and intensity of these diffuse segments.
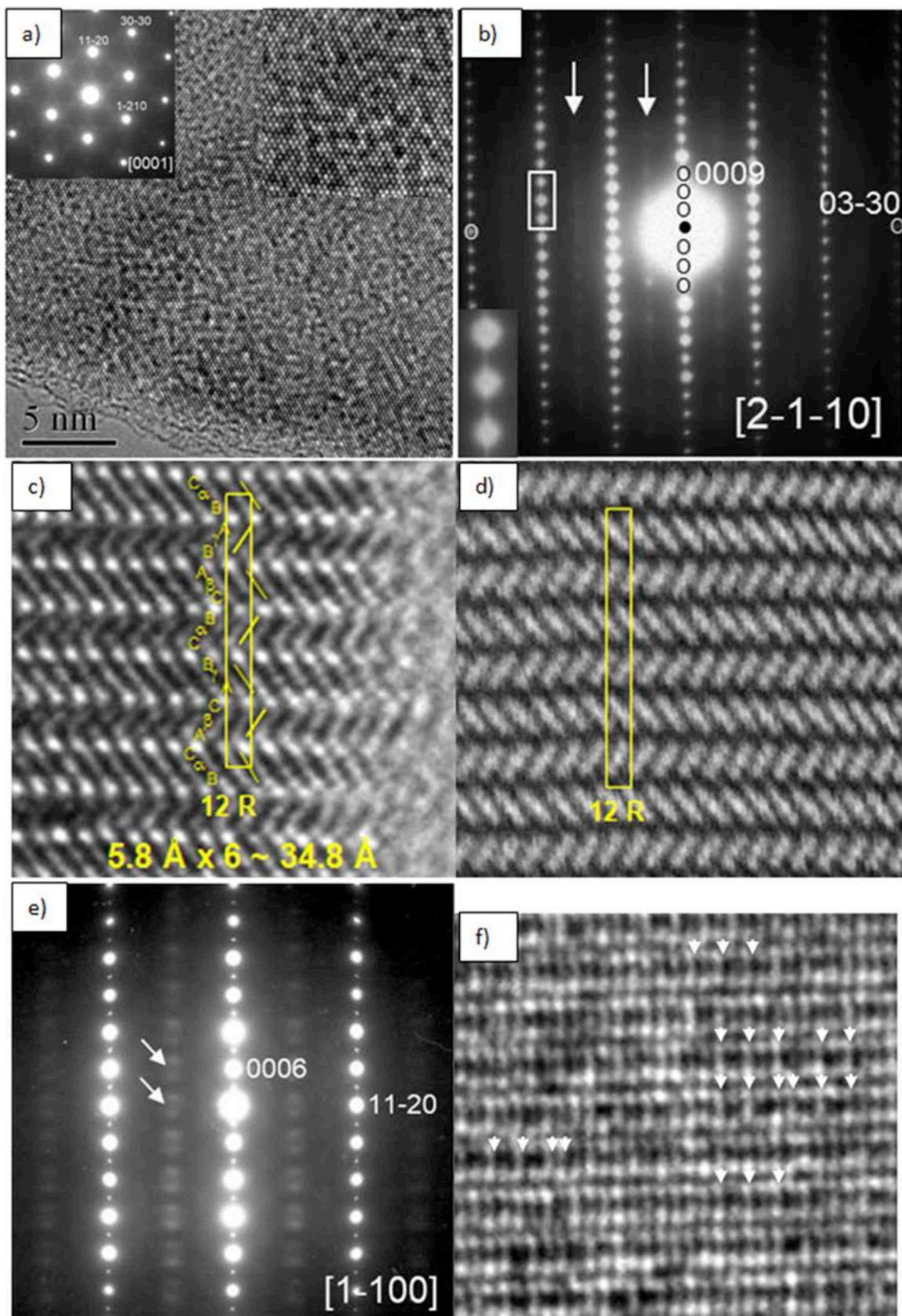
Fig. 8. (a) HRTEM image of 12R-$M_{1+x}S_2$ (with x ~ 0.21, M = Ge/Ti) taken along the *[0001]* zone axis; the insets show the corresponding SAED pattern and an enlargement of the micrograph, (b) *[2-1-10]* zone axis SAED pattern, the inset shows streaking running along *c**

among the main reflections; the arrows point to diffuse extra reflection rows; (c, d) Correspondi-ng HRTEM and HAADF-STEM images showing the 12R stacking sequence...aBαCbAγBc..; (e) *[1-100]* zone axis SAED pattern showing diffuse intensity along c* marked by arrows and assigned to short-range ordering of extra atoms and vacancies; (f) Corresponding HRTEM image, the arrows highlight a few small domains with a double periodicity along *[11-20]*.
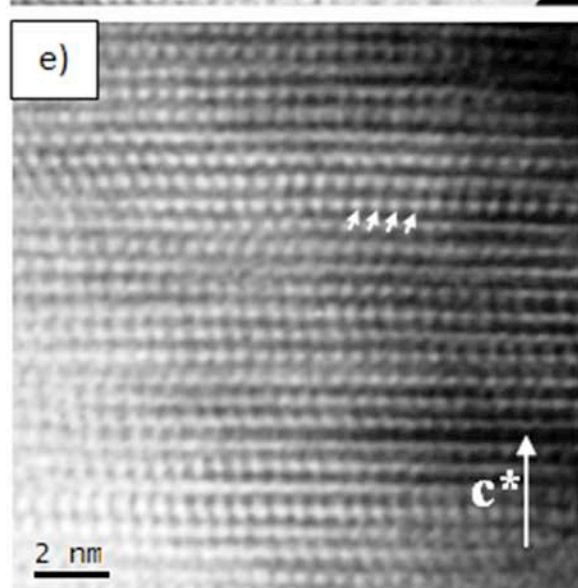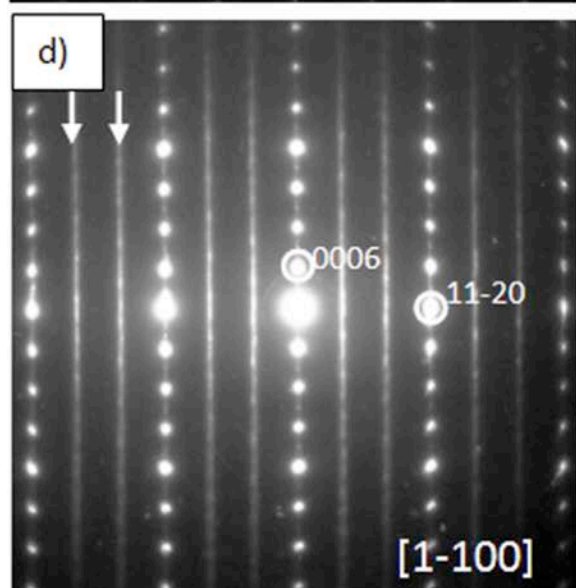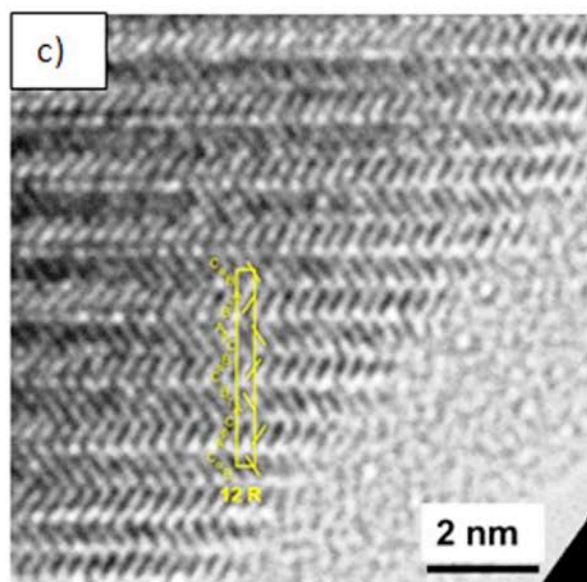
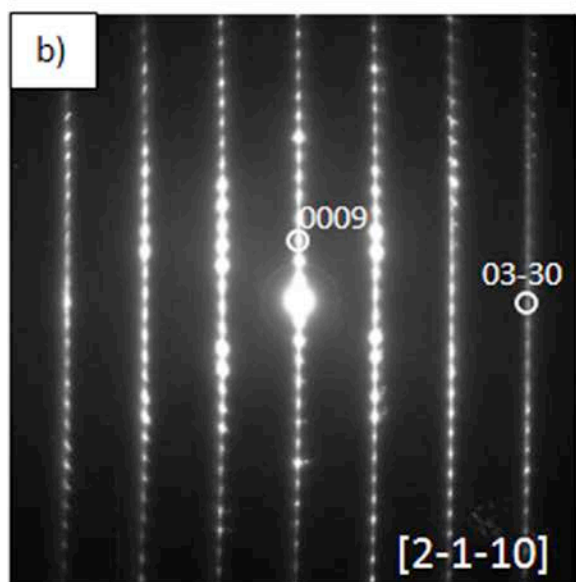a) [0001]

b) [2-1-10]
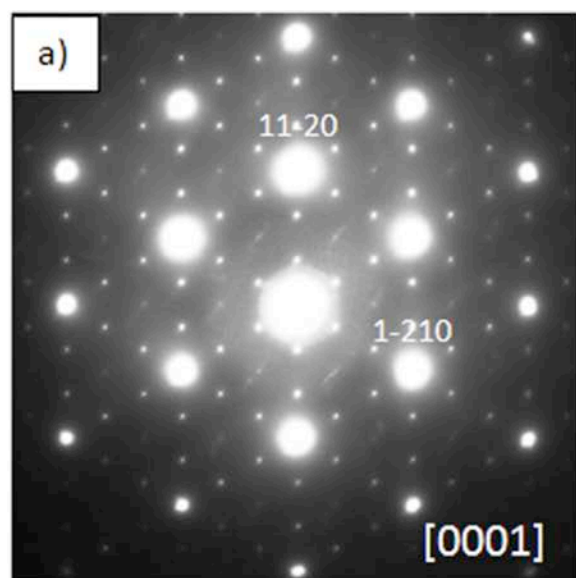
0009

03-30

c)

12 R

2 nm

d) [1-100]

0006

11-20

e)

c*

2 nm

Fig. 9. (a) SAED pattern of 12R-$M_{1+x}S_2$ (with x ~ 0.27, M = Ge/Ti) taken along the *[0001]* zone axis, notice the sharp satellite reflections running along *<11-20>**; (b) *[2-1-10]* zone axis SAED pattern; (c) HRTEM image taken along *[2-1-10]* zone axis; (d) *[1-100]* zone axis SAED pattern showing diffuse intensity along c* marked by arrows and assigned to short-range ordering of extra atoms and vacancies; (e) Corresponding HRTEM image, the arrows highlight a threefold order along [11-20]*, i.e. $\sqrt{3}a$; notice the disorder along the stacking direction *c**.